

## Photochromism of three photosensitive Fe centers in SrTiO<sub>3</sub>

R. L. Berney\* and D. L. Cowan

*Department of Physics, University of Missouri, Columbia, Missouri 65211*

(Received 17 March 1980)

Three paramagnetic Fe defect complexes have been observed by electron-spin resonance in chemically reduced crystals of SrTiO<sub>3</sub>. These are identified as (1) an Fe<sup>3+</sup> ion substituted on a Ti site with a nearby charge-compensating interstitial impurity, and (2) and (3) two charge states of substitutional Fe with a near-neighbor oxygen vacancy, Fe<sup>2+</sup>-V<sub>0</sub> and Fe<sup>1+</sup>-V<sub>0</sub>. These three defects are related in the sense that photoexcitation can reversibly switch electrons between the vacancy-associated and interstitial-associated sites. An analysis of the response to polarized light, and of the kinetics of charge transfer, shows that in both the forward and reverse directions of optical pumping the mobile charge carrier is a valence-band hole. Four distinct charge states of the Fe-V<sub>0</sub> system have now been identified, and the relative instability of SrTiO<sub>3</sub> toward formation of multiple-impurity charge states is briefly discussed.

### I. INTRODUCTION

SrTiO<sub>3</sub> is one of a number of transition-metal oxides that form in the ABO<sub>3</sub> perovskite structure. It is a diamagnetic insulator with a 3.2-eV band gap separating the oxygen 2*p* valence band from the empty titanium 3*d* conduction band, and it is a reasonable first approximation to consider the binding as primarily ionic.

When the pure crystal is doped with iron-group impurities they are known to enter substitutionally on the titanium site, for reasons related to ionic size. These impurity ions are then either octahedrally coordinated with six near-neighbor oxygens, or charge compensated with a near-neighbor oxygen vacancy (V<sub>0</sub>) along one of the [100] directions in the cubic Ti-centered unit cell. Some examples that have been studied by ESR include Fe<sup>3+</sup>,<sup>1</sup> Mn<sup>2+</sup>,<sup>2</sup> Fe<sup>3+</sup>-V<sub>0</sub>,<sup>3,4</sup> Ni<sup>3+</sup>-V<sub>0</sub>,<sup>5</sup> and Mn<sup>2+</sup>-V<sub>0</sub>.<sup>2</sup> Many of these doped crystals show interesting photochromic properties that make them at least potentially useful for device applications.<sup>6-8</sup>

Fe has probably been studied more thoroughly as an impurity in these crystals than any other ion. ESR, optical, and electrical studies have shown a remarkable variety of charge states are available to the impurity systems. In addition to the Fe<sup>3+</sup> and Fe<sup>3+</sup>-V<sub>0</sub> centers cited above, an optical-absorption band has been identified as belonging to Fe<sup>4+</sup> in an "as-grown" crystal.<sup>6</sup> In samples that have been oxidized by heat treating in air both Fe<sup>4+</sup>-V<sub>0</sub> (Ref. 9) and Fe<sup>5+</sup> (Ref. 10) appear, as well as a partially identified Fe<sup>5+</sup> (Ref. 11) system in a noncubic site.

This paper presents ESR and optical results for several Fe-defect complexes in "as-grown" SrTiO<sub>3</sub> and in SrTiO<sub>3</sub> crystals which have been chemically reduced by heating in a hydrogen atmosphere at high temperature. After the heat treatment we find a sim-

ple optically induced charge transfer sequence in which an electron can be reversibly switched between two distinct Fe-associated defect sites. One of these sites is the Fe-V<sub>0</sub> system, the other site is not fully characterized here but we believe it involves an interstitial near a normal substitutional Fe, and this site will be labeled Fe-*I*.

Since the electron transfer leads to two distinct charge states at each of two sites, four impurity species participate in the optical cycling. Three of these are directly observed by ESR. An outline of our observations is as follows: We begin with SrTiO<sub>3</sub> crystals grown by National Lead and doped with approximately 80 ppm Fe. ESR of these "as-grown" crystals shows the well-known Fe<sup>3+</sup> and Fe<sup>3+</sup>-V<sub>0</sub> centers, and the new interstitial system Fe<sup>3+</sup>-*I*. The relative position of these centers in the 3.2-eV band gap is shown in Fig. 1(a). When these crystals are heated to ≈ 1100 K in hydrogen and then quenched, oxygen vacancies are introduced into the sample. These vacancies act as shallow donors, and their introduction will cause the Fermi level to rise, as shown in Fig. 1(b). The crystal is now in an optically activated state. The vacancy system contains a substantial number of Fe<sup>2+</sup>-V<sub>0</sub> centers, and all of the interstitial sites have gained an electron, converting them into (Fe<sup>3+</sup>-*I* + *e*). This last complex shows no ESR spectrum, so the precise location of the extra electron is undetermined. For convenience in notation we call it Fe<sup>2+</sup>-*I*. If the crystal is now cooled and illuminated with blue light, an electron is driven out of the valence band and into the Fe<sup>2+</sup>-V<sub>0</sub> system, converting it into Fe<sup>1+</sup>-V<sub>0</sub>. The valence-band hole is captured by the Fe<sup>2+</sup>-*I* system, regenerating the Fe<sup>3+</sup>-*I* seen before heat treatment. These new charge states are stable indefinitely at temperatures below about 200 K, but illuminating the sample with ir light erases both optically produced charge states and re-

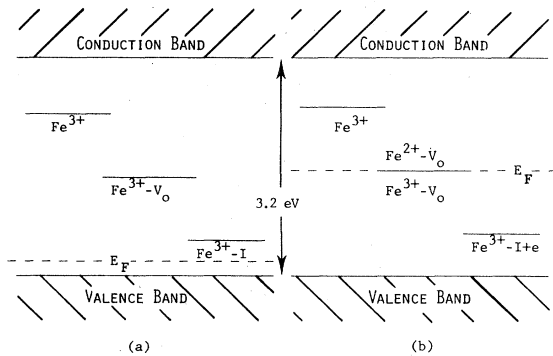


FIG. 1. (a) Impurity level diagram and Fermi level in the as-grown crystals. (b) The same diagram in reduced samples, showing the Fermi level pinned at the  $\text{Fe}^{3+}-V_0$  site.

stores the crystal to its original condition.

In Sec. II we present the ESR results for the three new centers  $\text{Fe}^{3+}-I$ ,  $\text{Fe}^{2+}-V_0$ , and  $\text{Fe}^{1+}-V_0$ .<sup>12</sup> Section III describes the optical results, including some polarization sensitive pumping effects that allows us to develop a microscopic model of the charge transfer process. Measurements involving the kinetics of the optical pumping confirm this model. Finally, in Sec. IV, we give some limited analysis of three separate aspects of the data. The first of these is the polarization dependent response to the optical pumping. Our tentative conclusion is that the polarization effects can be adequately explained by considering the  $\text{Fe}-V_0$  system as a small molecular cluster with charge transfer bands. Secondly, the ESR spin-Hamiltonian parameters are now available for four separate charge states of the  $\text{Fe}-V_0$  system (from  $\text{Fe}^{4+}-V_0$  to  $\text{Fe}^{1+}-V_0$ ). In a naive crystal-field model this would represent four different ions in the same crystal field. We briefly discuss the extent to which this naive approximation can hold true, and how well it can be tested. The third and last topic is a short discussion of the unusual appearance of four distinct charge states of the  $\text{Fe}-V_0$  complex, all clustered within the 3.2-eV band gap of the  $\text{SrTiO}_3$  crystal.

## II. ESR RESULTS

All the ESR measurements described here were taken on an X-band microwave spectrometer of conventional design, operated either as a homodyne system with 100-kHz magnetic field modulation or as a superheterodyne system with a 30-MHz intermediate frequency. The spectrometer was normally tuned to the absorption mode.

The samples were cut along (100) planes and typically measured about  $1 \times 2 \times 3 \text{ mm}^3$ . They were mounted either at the center or along the wall of a

copper  $\text{TE}_{102}$  reflection cavity that was slotted to pass an optical pumping beam.

The low-frequency dielectric constant of  $\text{SrTiO}_3$  is so large ( $\epsilon/\epsilon_0 \approx 300$  at room temperature, and varying as  $1/T$  with temperature) that even these small samples significantly perturb the cavity modes, particularly at low temperature. "Good" low-temperature modes show effective filling factors an order of magnitude or so greater than those expected for an unperturbed cavity, and it was sometimes necessary to tune the temperature slightly to find a good, relatively stable mode. The uncertainty in effective filling factor produces a corresponding uncertainty in the absolute number of spins contributing to a particular signal, and even ratios of spins in two different centers observed simultaneously can be confounded by different microwave polarization selection rules for the two transitions, and our uncertainty about exact field configurations in the sample. This last problem was not particularly severe, though. Different selection rules were routinely checked, and were always in reasonable agreement with the expected behavior. In other words, we always knew the predominate direction of the microwave  $B$  field in the sample, if not its absolute magnitude.

### A. $\text{Fe}^{3+}-I$

Three ESR signals are observed at room temperature in the as-grown samples. Two of these are the well-known  $\text{Fe}^{3+}$  and  $\text{Fe}^{3+}-V_0$  defects, present in roughly comparable numbers for charge compensation.<sup>6,7</sup> The third spectrum consists of more than 20 sharp lines occurring over a 700- to 10 000-G range for some orientations of the applied magnetic field. A preliminary analysis of this spectrum was performed by comparison with the numerical results of Dowsing and Gibson,<sup>13</sup> who analyzed an  $S = \frac{5}{2}$  system in rhombic symmetry for a range of fine-structure constants  $D$  and  $E$ . The defect has been identified as an  $\text{Fe}^{3+}$  ion at a site of rhombic symmetry ( $\text{Fe}^{3+}-I$ ). The principle axes for the rhombic fine-structure tensor are parallel to the [100], [011], and  $[0\bar{1}1]$  crystal directions ( $x$ ,  $y$ , and  $z$ , respectively). This gives six inequivalent fine-structure ellipsoids of spin  $\frac{5}{2}$  for a maximum of 90 possible transitions at fixed magnetic field. When  $H_0$  (the applied magnetic field) is along a [100] direction, the six ellipsoids collapse into two degenerate groups, one with two ellipsoids and the other with four ellipsoids. If  $H_0$  is along the [110] direction four of the ellipsoids are equivalent and the other two are independent giving three inequivalent ellipsoids.

A spin Hamiltonian of the form

$$H = g\beta\vec{S}\cdot\vec{H} + D[S_z^2 - \frac{1}{3}S(S+1)] + E(S_x^2 - S_y^2) \quad (1)$$

with  $D = 0.27 \text{ cm}^{-1}$ ,  $E = 0.049 \text{ cm}^{-1}$ ,  $S = \frac{5}{2}$ , and

$g = g_e$  was numerically diagonalized for  $H_0$  parallel to the  $x$ ,  $y$ , or  $z$  principle axes as a function of  $H_0$ , giving the energy-level diagrams shown in Fig. 2. The vertical lines indicate observed  $X$ -band transitions at two microwave frequencies. The arrow near 4400 G marks a particularly interesting transition where an increase in microwave frequency moves the transition to lower field. Quantitatively, the experimentally measured slopes of  $\Delta H$  vs  $\Delta \nu$  for the observed transitions agree very well with those calculated from Eq. (1) at the two microwave frequencies of Fig. 2, although absolute field positions for some of the lines are in error by 100 to 200 G (see Table I). This discrepancy is probably due to the four fourth-order fine-structure terms omitted from the spin Hamiltonian of Eq. (1). An attempt at including these terms was made, but the computer time necessary to search this six-parameter space (two second- and four fourth-order fine-structure terms) was very great and the attempt was abandoned. However, reasonable fourth-order terms can easily produce shifts of a few hundred gauss.

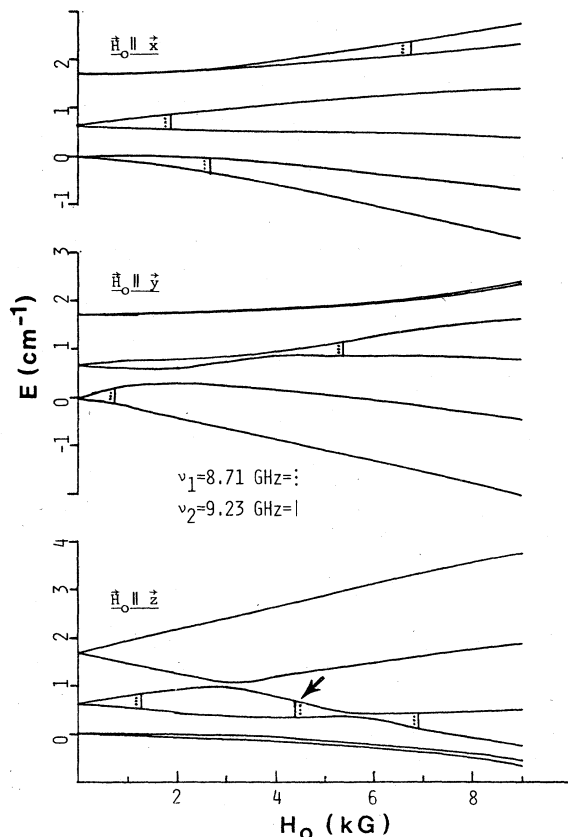


FIG. 2. Energy-level diagrams for  $\text{Fe}^{3+}\text{-I}$  with  $H_0$  parallel to the  $x$ ,  $y$ , and  $z$  principle axes. The solid lines indicate observed transitions at 9.23 GHz and the dotted lines indicate transitions observed at 8.71 GHz.

At 105 K  $\text{SrTiO}_3$  undergoes a structural phase change.<sup>4,14</sup> Viewed from a  $\text{Ti}^{4+}$  site this phase change can be simply described as a rigid rotation of the surrounding oxygen octahedron about a  $[100]$  axis, with a rotation angle of  $1.4^\circ$  at 77 K. To a good approximation the spin Hamiltonian of a paramagnetic ion at this site will be unchanged, except for a corresponding rotation in the principle axes of the fine-structure tensor (and the obvious complications because the sample is now multidomain). At a  $\text{Sr}^{2+}$  site (rare-earth ions will substitute here, for example) no such simple description is expected or observed. The  $\text{Fe}^{3+}\text{-I}$  signal at 77 K shows a rigid rotation of the fine-structure tensor by  $1.75 \pm 0.05^\circ$  indicating it is substitutional at a  $\text{Ti}^{4+}$  site.

The rhombic crystal field at the Fe site implies some nearby impurity or defect is perturbing the lattice. If this defect is located in a  $[110]$  direction then the principle axes of the fine-structure tensor are automatically as observed because of the  $(001)$  and  $(1\bar{1}0)$  reflection planes, and we also have a natural interpretation for the systems being nearly axial along  $[110]$ . The nearest lattice site in this direction is a Ti site situated  $2\sqrt{2}$  near-neighbor distances away. This seems much too remote to produce such a large perturbation. The natural interstitial position in  $\text{SrTiO}_3$  is also in the  $[110]$  direction from a Ti site though,  $\sqrt{2}$  near-neighbor distances away, and we believe this site is occupied by an impurity. Since  $\text{Na}^+$  is a major impurity in our samples ( $\approx 30$  ppm) it is a logical candidate, although on ionic size considerations a

TABLE I. The experimentally measured and calculated turning points for  $\text{Fe}^{3+}\text{-V}_0$  are listed in the first two columns for  $H_0$  along the principle axes. The calculated values are from Eq. (1) with  $D = 0.27 \text{ cm}^{-1}$ ,  $E = 0.049 \text{ cm}^{-1}$ ,  $g = g_e$ , and  $\nu = 9.223 \text{ GHz}$ . The last two columns are experimental and calculated shifts in field position as the frequency is changed from 8.701 to 9.233 GHz. All measurements in gauss.

Field position		Shift in field position	
$H_0$ (expt)	$H_0$ (calc)	$\Delta H_0$ (expt)	$\Delta H_0$ (calc)
[100]	$H_0$ along $x$	[100]	$H_0$ along $x$
1909	1962	116	120
2850	2798	NA	135
6857	6669	195	200
[0 $\bar{1}$ 1] and [011]	$H_0$ along $y$	[0 $\bar{1}$ 1] and [011]	$H_0$ along $y$
728	740	40	45
5403	5490	98	105
	$H_0$ along $z$		$H_0$ along $z$
1262	1285	72	70
4410	4417	-70	-75
6870	6915	70	70

Na<sup>+</sup> ion would be rather cramped. Li<sup>+</sup> would easily fit in this interstitial site, but we have no direct evidence that Li is present at the several ppm levels required. In either case, the net negative effective charge of an Fe<sup>3+</sup> ion at a Ti site would tend to attract an interstitial alkali ion and produce an electrically neutral defect. The analysis of the kinetics in Sec. III does suggest overall electrical neutrality for this defect.

### B. Fe<sup>2+</sup>-V<sub>0</sub>

Crystals treated at high temperature ( $\approx 1100$  K) in a hydrogen atmosphere and quenched show a large decrease in the concentration of Fe<sup>3+</sup>-V<sub>0</sub>, the disappearance of the Fe<sup>3+</sup>-I signal, and the appearance of new axially symmetric transitions at both very high and very low magnetic fields ( $\approx 10\,500$  and  $\approx 800$  G, respectively). These signals are both due to Fe<sup>2+</sup>-V<sub>0</sub> ( $S=2$ ,  $3d^6$ ) created by the addition of an electron to the Fe<sup>3+</sup>-V<sub>0</sub> defects as the Fermi level was raised by the reducing treatment.

Figure 3 shows room-temperature data for  $H_0$  in a (001) plane. The high-field lines are  $\approx 200$  G wide and arise from transitions between the  $|\pm 1\rangle$  states of the  $S=2$  system. The intensity of these signals is a maximum when  $H_0$  is perpendicular to the defect

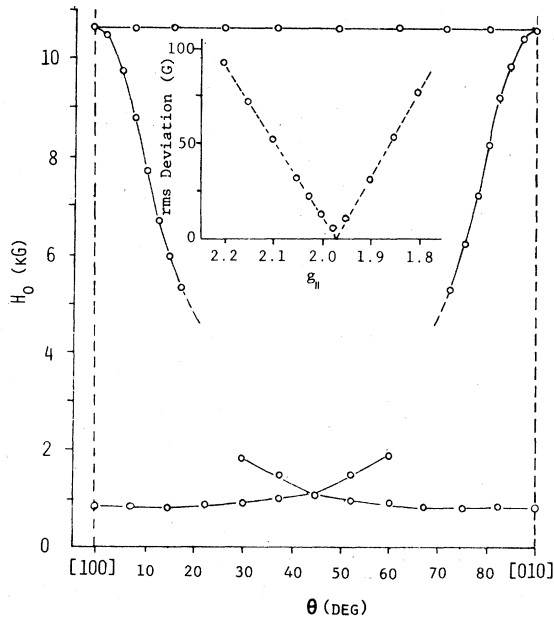


FIG. 3. Calculated and measured resonance fields for Fe<sup>2+</sup>-V<sub>0</sub>. Only a few data points are shown for clarity. Error bars on the data are smaller than the thickness of the line. The low-field lines are calculated from Eq. (5), (the  $|\pm 2\rangle$  transitions); and the high-field lines are calculated from Eq. (3) (the  $|\pm 1\rangle$  transitions). The inset is a least-squares analysis of the high-field transition as a function of  $g_{\parallel}$ .

axis and decreases rapidly as  $H_0$  rotates away from perpendicular. The low-field lines are  $\approx 20$  G wide and arise from transitions between the  $|\pm 2\rangle$  states of the  $S=2$  system. These signals have maximum intensity when  $H_0$  is parallel to the defect axis. The intensity decreases as  $H_0$  rotates away from parallel.

Both of these systems may be described by a spin Hamiltonian of the form

$$H = \beta \vec{S} \cdot \vec{g} \cdot \vec{H} + D [S_z^2 - \frac{1}{3} S(S+1)] + \frac{1}{48} a (S_x^4 + S_y^4) \quad (2)$$

with  $D = +9.58 \text{ cm}^{-1}$ ,  $a = 0.046 \pm 0.02 \text{ cm}^{-1}$ , and  $S=2$ . In zero magnetic field with  $D \gg a$  the five spin states split into three levels, with the  $|\pm 1\rangle$  levels degenerate at an energy  $D$  above the  $|0\rangle$  level, and the  $|\pm 2\rangle$  levels nearly degenerate and at an energy  $3D$  above the  $|\pm 1\rangle$  levels. Perturbation theory on the  $|\pm 1\rangle$  levels when  $H_0$  is perpendicular to the  $z$  axis of the system yields<sup>15(a)</sup>

$$E_{|1^s\rangle} = D + \frac{3(g_{\perp}\beta H)}{D} - \frac{(g_{\perp}\beta H)}{3D + \frac{1}{2}a[\cos(4\phi)]} \quad (3)$$

$$E_{|1^a\rangle} = D - \frac{(g_{\perp}\beta H)}{3D - \frac{1}{2}a[\cos(4\phi)]}$$

where the states are  $|1^s\rangle = (1/\sqrt{2})(|+1\rangle + |-1\rangle)$  and  $|1^a\rangle = (1/\sqrt{2})(|+1\rangle - |-1\rangle)$ . The energy difference between these is

$$\Delta E = \frac{3(g_{\perp}\beta H)^2}{D} \left[ 1 + \frac{a[\cos(4\phi)]}{270} \right] \quad (4)$$

At 9.3 GHz  $\Delta E = h\nu = 0.31 \text{ cm}^{-1}$ , and for  $H \approx 10\,500$  G,  $g \approx 2.0$ , Eq. (4) gives  $D \approx 10 \text{ cm}^{-1}$ . A transition between these levels is allowed because the  $|1^s\rangle$  and  $|1^a\rangle$  states are coupled by the  $z$  component of  $H_{rf}$ . This polarization selection rule has been verified.

As  $H_0$  is rotated away from perpendicular the  $|1^s\rangle$  and  $|1^a\rangle$  states rapidly change into  $|+1\rangle$  and  $|-1\rangle$  states which are not coupled by any component of  $H_{rf}$  and the transition intensity disappears. The transitions can be followed far enough to make a reasonable estimate of  $g_{\parallel}$  possible. The solid lines of Fig. 3, showing the angular behavior of the  $|\pm 1\rangle$  transitions, were generated by a computer solution of the spin Hamiltonian of Eq. (2). The inset shows a least-squares fit to the data as a function of  $g_{\parallel}$ . The fit is insensitive to the value of  $a$ .

The low-field transitions arise from the admixtures of the  $|\pm 2\rangle$  states by the  $a$  term of Eq. (2) and may be described by the same equation that was used for the  $|\pm 2\rangle$  transitions of the Fe<sup>4+</sup>-V<sub>0</sub> system.<sup>9</sup> This equation may be written

$$\Delta E_{|\pm 2\rangle} = [(4g_{\parallel}\beta H_0 \cos\theta) + a^2]^{1/2} \quad (5)$$

The solid lines of Fig. 3 for the  $|\pm 2\rangle$  transitions are from Eq. (5) with  $a = 0.046 \pm 0.02 \text{ cm}^{-1}$  and  $g_{\parallel} = 1.97$ , the  $g_{\parallel}$  value that best fit the  $|\pm 1\rangle$  transitions. The  $|\pm 2\rangle$  transitions are predicted to have maximum intensity when the  $z$  axis of the defect, the  $H_{rf}$  field, and the  $H_0$  field all are parallel. In practice it turned out to be essential to satisfy this unusual geometrical constraint in order to observe the signal.

The sign of  $D$  was determined by observing the signals at 4.2 K. The  $|\pm 2\rangle$  signal was completely gone, but the  $|\pm 1\rangle$  signal was still observable. A positive  $D$  has the  $|\pm 2\rangle$  states  $\approx 40 \text{ cm}^{-1}$  above the ground  $|0\rangle$  state causing them to be depopulated at 4.2 K, whereas the  $|\pm 1\rangle$  states are only  $\approx 10 \text{ cm}^{-1}$  from the  $|0\rangle$  state and will still be weakly populated as observed.

The  $|\pm 1\rangle$  and  $|\pm 2\rangle$  signals may be shown to arise from the same defect in several ways. (1) Both signals appear together. Only in the reduced samples where the  $|\pm 1\rangle$  signal appears, will the  $|\pm 2\rangle$  signal appear. (2) The structural phase change shows the same rotation angle of  $\approx 1^\circ$  at 77 K for both. (3) The intensity of the  $|\pm 2\rangle$  transition as compared to the  $|\pm 1\rangle$  transition may be used to calculate a value for  $a$ . The value of  $a$  calculated in this manner is  $a = 0.028 \text{ cm}^{-1}$ , which is within the experimental limits of  $a$  as calculated from the field position. (4) Finally, the order of magnitude difference in the linewidths for these  $|\pm 1\rangle$  and  $|\pm 2\rangle$  transitions is consistent with their having similar relaxation times. This relaxation time may be loosely related to the homogeneous linewidth (e.g., through the Bloch equations) by<sup>15(b)</sup>

$$\frac{1}{\tau_2'} = \frac{\sqrt{3}}{2} \delta\omega = \frac{\sqrt{3}}{2} \frac{g^{\text{eff}} \beta \Delta H}{\hbar} \quad (6)$$

For the  $|\pm 2\rangle$  transition  $g^{\text{eff}} = 8.0$  and  $\Delta H \approx 20 \text{ G}$  and for the  $|\pm 1\rangle$  transition  $g^{\text{eff}} = 1.2$  and  $\Delta H \approx 200 \text{ G}$  giving (in  $10^9 \text{ sec}^{-1}$ )

$$\frac{1}{\tau_2'} = \begin{cases} \frac{\sqrt{3}}{2} \frac{8(\beta)20}{\hbar} = 1.2 & \text{for } |\pm 2\rangle \\ \frac{\sqrt{3}}{2} \frac{1.2(\beta)200}{\hbar} = 1.8 & \text{for } |\pm 1\rangle \end{cases} \quad (7)$$

$$\frac{1}{\tau_2'} = \begin{cases} \frac{\sqrt{3}}{2} \frac{1.2(\beta)200}{\hbar} = 1.8 & \text{for } |\pm 1\rangle \\ \frac{\sqrt{3}}{2} \frac{8(\beta)20}{\hbar} = 1.2 & \text{for } |\pm 2\rangle \end{cases} \quad (8)$$

Thus, the order of magnitude difference in linewidth reflects similar relaxation rates for both signals.

The relaxation time for both the  $|\pm 1\rangle$  and  $|\pm 2\rangle$  lines is the order of  $6 \times 10^{-10} \text{ sec}$ . This would be a very short relaxation time if the ion were a Kramers ion. On the other hand, it is a fairly long time for a non-Kramers system. Tinkham has observed an  $\text{Fe}^{2+}$  ion in tetragonal symmetry in  $\text{ZnF}_2$  where the signal could only be observed below  $\approx 90 \text{ K}$  because of line broadening.<sup>16</sup> However, his signal had a  $g_{\parallel}^{\text{eff}} = 2g_{\parallel} = 8.98$  for the  $S_z = \pm 2$  doublet, indicating a much stronger orbital coupling. Kaufmann has observed

non-Kramers  $\text{Fe}^{2+}$  and  $\text{Fe}^{4+}$  signals in  $\text{CdSiP}_2$  both of which can still be observed at room temperature.<sup>17</sup>

Spin-Hamiltonian parameters for this system can be determined from the crystal-field analysis as given by Griffith,<sup>18</sup> with all calculations limited to the  $^5D$  ground state of the high-spin  $\text{Fe}^{2+}$  ion. The octahedral field splits this ground  $^5D$  into a  $^5E$  and  $^5T_2$  with the  $^5T_2$  going low. The axial field further splits the  $^5E$  state into two singlets and the  $^5T_2$  states into a singlet and doublet (see Fig. 4). The perturbation Hamiltonian to be used in these 25 ground states is

$$H = \lambda \bar{L} \cdot \bar{S} + \beta \bar{H} \cdot (\bar{L} + 2\bar{S}) \quad (9)$$

the spin-orbit coupling, and the Zeeman terms, respectively.

A perturbation calculation within the 25 states of the  $^5D$  then yields for the lowest-lying levels of  $^5B_2$

$$D = \frac{\lambda^2}{W_1} - \frac{4\lambda^2}{W_2} \quad (10)$$

$$g_{\parallel} = 2 - 3 \left[ \frac{\lambda}{W_1} \right]^2 + \frac{8|\lambda|}{W_2}$$

where  $W_1$  is the energy splitting to the  $^5E$ , and  $W_2$  is the splitting to the  $^5B_1$ . On physical grounds this last state is expected to be very high in energy, somewhere between 15 000 and 40 000  $\text{cm}^{-1}$ . A solution to Eqs. (10) with  $W_2$  in this range requires  $72 < |\lambda| < 82 \text{ cm}^{-1}$ . Since this corresponds to a very reasonable orbital quenching of some 20% from the

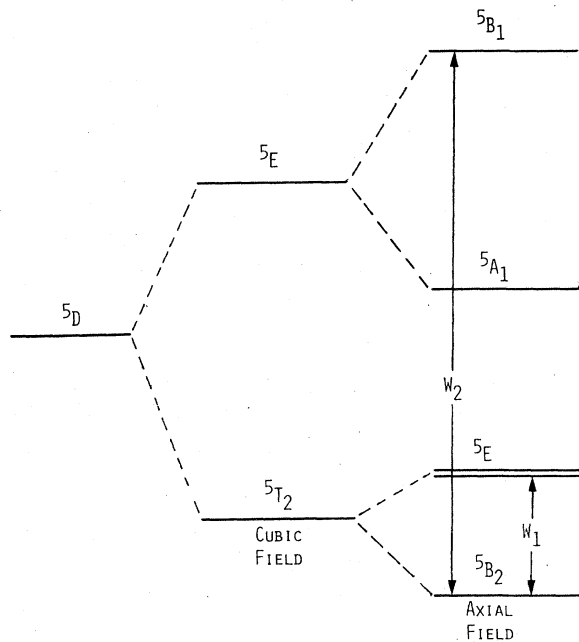


FIG. 4. Energy-level diagram for the ground state of a  $3d^6$  ion in both cubic and axial symmetry.

free-ion value for  $\lambda$  ( $\approx -100 \text{ cm}^{-1}$ ), Eqs. (10) seem completely consistent.  $W_1$  must be about  $800 \text{ cm}^{-1}$ . The expression for  $g_{\parallel}$  then gives 1.97 in excellent agreement with experiment.

### C. $\text{Fe}^{1+}\text{-}V_0$

A metastable ESR signal is observed in the reduced samples exposed to subband-gap light at low temperature ( $< 230 \text{ K}$ ). This signal has been identified as  $\text{Fe}^{1+}\text{-}V_0$  created from  $\text{Fe}^{2+}\text{-}V_0$  defects by the optical charge transfer of a valence electron onto the  $\text{Fe}^{2+}\text{-}V_0$  defect.<sup>12</sup> Figure 5 shows the angular behavior of the signal as  $H_0$  is rotated in a (001) plane. These signals are characteristic of transitions between  $S_z = \pm \frac{1}{2}$  levels of an  $S = \frac{3}{2}$  ion which is orbitally nondegenerate in a strong tetragonal field along the [100] direction.

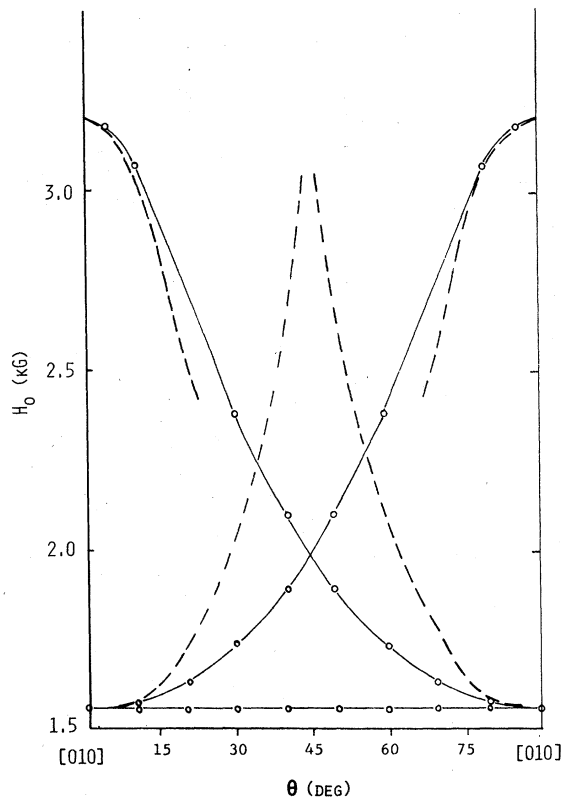


FIG. 5. Calculated and measured resonance fields for  $\text{Fe}^{1+}\text{-}V_0$ . Only a few data points are shown for clarity. Error bars on the data are smaller than the linewidth. The solid lines are calculated from Eq. (12), the  $|\pm \frac{1}{2}\rangle$  transition of an  $S = \frac{3}{2}$  system in a strong tetragonal field. The dashed lines represent the  $|\pm \frac{1}{2}\rangle$  transitions for the alternative model of an  $S = \frac{5}{2}$  system in a moderate tetragonal field ( $D = 0.12 \text{ cm}^{-1}$ ).

A spin Hamiltonian of the form

$$H = \beta \vec{S} \cdot \vec{g} \cdot \vec{H} + D [S_z^2 - \frac{1}{3} S(S+1)] \quad (11)$$

with  $D \gg h\nu$  will give<sup>3</sup>

$$g^{\text{eff}} = [g_{\parallel}^2 + (4g_{\perp}^2 - g_{\parallel}^2) \sin^2 \theta]^{1/2} \quad (12)$$

for the effective spin  $S_z = \pm \frac{1}{2}$  Kramers pair. The solid lines of Fig. 5 represent  $S = \frac{3}{2}$ ,  $g_{\parallel} = 1.999$ , and  $g_{\perp}^2 = 2g_1 = 4.116$  ( $g_1 = 2.058$ ). Again measurements below the structural phase transition show the defect is at a  $\text{Ti}^{4+}$  site with a rotation angle of  $0.95 \pm 0.05^\circ$  at  $77 \text{ K}$ . The phase transition also has the effect of inducing a term in the spin Hamiltonian of Eq. (11) of the form

$$E(S_x^2 - S_y^2) \quad (13)$$

By observing the splitting of the lines when  $H_0$  is perpendicular to the  $z$  axis of the defect it is possible to measure  $|E/D|$ . For  $\text{Fe}^{1+}\text{-}V_0$  this is  $|E/D| = 10.5 \pm 0.2 \times 10^{-4}$  as compared to  $|E/D| = 9.6 \times 10^{-4}$  for  $\text{Fe}^{3+}\text{-}V_0$ .<sup>14</sup>

The energy levels for the  $S = \frac{3}{2}$  state of  $\text{Fe}^{1+}$  ( $3d^7$ ) in a strong tetragonal field are shown in Fig. 6. Abragam and Pryce<sup>19</sup> have analyzed the low-lying levels of this system for  $g_{\parallel}$  and  $g_{\perp}$ . These two measured quantities are a function of four parameters ( $\lambda, W, \gamma, K$ ) where  $\lambda$  is the spin-orbit coupling,  $W$  is the energy splitting between the  ${}^4A_2$  and  ${}^4E$  levels of the  ${}^4T_{1g}$  state,  $\gamma$  is used to satisfy the weak- or strong-field limit with  $\gamma = -\frac{3}{2}$  for the weak-field limit and  $\gamma = -1$  for the strong-field limit, and  $K$  is the orbital quenching. Assuming reasonable values for  $\lambda$  ( $\approx -120 \text{ cm}^{-1}$ , the free-ion value),  $K$  ( $= 0.8$ , a 20%

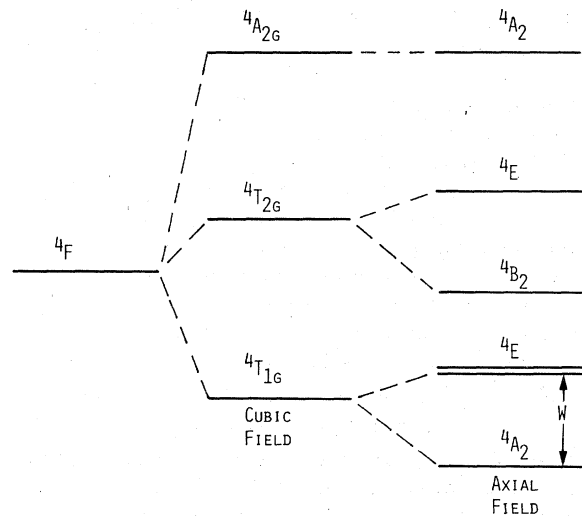


FIG. 6. Energy-level diagram for the ground state of  $3d^7$  ion in both cubic and axial symmetry.

spin-orbit reduction), and  $\gamma$  ( $= -1.3$ , an intermediate field), a  $W$  of  $+3500 \text{ cm}^{-1}$  yields  $g_{\parallel} = 1.998$  and  $g_{\perp}^1 = 2g_{\perp} = 4.118$  successfully accounting for both the small negative  $\delta g_{\parallel}$  and the large positive  $\delta g_{\perp}$ .

#### D. Alternative models

The defects identified as  $\text{Fe}^{2+}\text{-}V_0$  and  $\text{Fe}^{1+}\text{-}V_0$  owe their identification to several factors. (1) The intensity of the signals excludes any impurity other than Fe as the source of the signals. (2) The rotation angles below the phase transition ( $\approx 1^\circ$  for both) are consistent with all other vacancy associated defects for which a rotation angle is known.<sup>3,5,9</sup> (3) Reduction of the crystals tends to raise the Fermi level and lower the valence states of the Fe impurities, just as oxidation tends to lower the Fermi level and increase the valence states of the impurities.

The only plausible alternative model with  $S = \frac{3}{2}$  would be  $\text{Fe}^{5+}\text{-}V_0$  ( $3d^3$ ). This charge state would be  $+3$  with respect to the crystal lattice, an absurd result. The  $g$  shifts observed are incompatible with a  $d^3$  ion in any case. The only other  $S = 2$  system available is  $\text{Fe}^{4+}\text{-}V_0$  ( $3d^4$ ), but this defect has previously been identified<sup>9</sup> in oxidized samples and shows a positive  $g$  shift and a cubic fine-structure constant three times larger than the  $S = 2$  system described in this paper. It is clear the vacancy-associated Fe defects we observe must represent the addition of electrons to the  $\text{Fe}^{3+}\text{-}V_0$  system first by reduction and then by optical excitation. This same charge transfer sequence has been observed in Ni-doped samples of  $\text{SrTiO}_3$  by Müller *et al.*<sup>5</sup>

There might be some question as to whether the extra electrons are associated with the Fe ion ( $\text{Fe}^{2+}\text{-}V_0$  and  $\text{Fe}^{1+}\text{-}V_0$ ), or the vacancy ( $\text{Fe}^{3+}\text{-}V_0 + e$  and  $\text{Fe}^{3+}\text{-}V_0 + 2e$ ). The  $S = 2$  system could then result from exchange coupling of the  $S = \frac{1}{2}$  electron in the vacancy with the  $S = \frac{5}{2}$   $\text{Fe}^{3+}$  ion giving an even-spin  $S = 2$  or  $S = 3$  system. It is difficult to completely eliminate this interpretation in the absence of an explicit description of the assumed vacancy-associated electron. There is no indication in the data, though, of any signal that could belong to an  $S = 3$  system, and the measured  $g$  shift would be hard to explain with an exchange-coupled complex. The case against the  $\text{Fe}^{3+}\text{-}V_0 + 2e$  interpretation is much stronger. The two electrons in the vacancy would certainly be coupled low spin ( $S = 0$ ), leaving us with a  $S = \frac{5}{2}$  system. The question then is whether the assignment of  $S = \frac{3}{2}$  to the data of Fig. 5 is completely unambiguous, or whether an  $S = \frac{5}{2}$  system in an appropriate crystal field might mimic the observed behavior. By choosing a weak tetragonal field ( $D \approx 0.12 \text{ cm}^{-1}$ ) it is in fact possible to get the observed  $g_{\perp}$  with an  $S = \frac{5}{2}$  ion, but a complete calculation, as illustrated by the dashed lines in Fig. 5, shows that the angular

dependence is all wrong. In fact, the  $g_{\perp}$  lines do not even smoothly connect with the  $g_{\parallel}$  lines. Finally, the observed  $g$  shifts for the  $\text{Fe}^{1+}\text{-}V_0$  ( $3d^7$ ) interpretation are consistent with the unusual experimental result of  $\delta g_{\parallel}$  negative and  $\delta g_{\perp}$  positive.

### III. PHOTOCROMISM

#### A. Production and decay model

The photochromic creation of  $\text{Fe}^{1+}\text{-}V_0$  has a broad spectral response with the entire visible spectrum contributing to the production. The maximum quantum efficiency for the production of the  $\text{Fe}^{1+}\text{-}V_0$  signal lies near 600 nm, where a rough calibration of absolute light intensity and absolute ESR signal indicates the excitation efficiency is nearly unity in our  $\approx 1\text{-mm}$ -thick samples. Assuming direct excitation of a valence electron into an  $\text{Fe}^{2+}\text{-}V_0$  center, the corresponding oscillator strength must be of the order of  $f \geq 0.1$ . The  $\text{Fe}^{3+}\text{-}I$  signal, which disappeared upon reduction, is recreated as the  $\text{Fe}^{1+}\text{-}V_0$  signal is produced. The two centers show a one to one correspondence in the rates of their production.

The metastable excited states produced by illumination with visible light will thermally decay above  $\approx 230 \text{ K}$ , but below this temperature the signals are stable. Illumination of the sample with ir light will erase both states together.

We believe these induced defect states are connected with a simple electron transfer between the two sites, and our model is shown in Fig. 7. Both the "write" signal with visible light, and the "erase" signal with ir light involve direct excitation of an electron out of the valence band and into the local de-

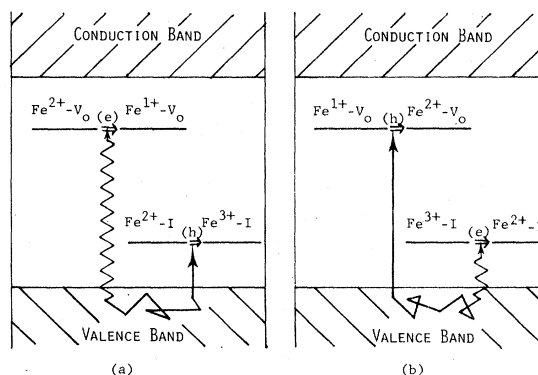


FIG. 7. (a) A model for the photochromic creation of  $\text{Fe}^{1+}\text{-}V_0$  by the direct excitation of a valence electron onto  $\text{Fe}^{2+}\text{-}V_0$  and subsequent hole migration and capture by  $\text{Fe}^{2+}\text{-}I$ , producing  $\text{Fe}^{3+}\text{-}I$ . (b) The reverse process, where both  $\text{Fe}^{1+}\text{-}V_0$  and  $\text{Fe}^{3+}\text{-}I$  are photochromically erased by a direct electron excitation and hole migration.

fect, with subsequent migration and capture of the valence-band hole. The evidence for this particular pattern rests on polarization sensitive excitation for the optical production process, and on analysis of the kinetics for the inverse optical decay process.

### B. Polarized production experiments and model

The most interesting feature of the optical production is the polarization dependence of the  $\text{Fe}^{1+}\text{-}V_0$  signal, which shows a preferential population of geometrically inequivalent defects depending on the orientation of the defect axis with respect to the electric field vector of the incident light.

In a typical experiment, we can align the magnetic field to examine the production of  $\text{Fe}^{1+}\text{-}V_0$  centers oriented along the  $x$  axis and along the  $y$  axis simultaneously. If the sample is now illuminated with  $z$ -polarized light, both orientations must be produced at the same rate, as observed. If the polarization of the incident light is along the  $x$  axis, however, we find an excess production of  $x$ -axis-oriented  $\text{Fe}^{1+}\text{-}V_0$  with blue light, and a deficiency with green light.

The polarization experiment was performed by observing the two  $g_1 \approx 4$  signals of the  $\text{Fe}^{1+}\text{-}V_0$  under a  $10^\circ$  rotation of  $H_0$  from a  $[100]$  crystal axis. With this rotation the signals are split by  $\approx 10$  G allowing their intensities to be monitored independently. The ESR trace of Fig. 8(a) shows these two lines pro-

duced by optical pumping at 400 nm with light polarized such that the polarization vector is perpendicular to both defect  $z$  axes.

Before converting these ESR signal ratios to population ratios though, we need to correct for the different microwave transition probabilities for the two geometries. With the static  $H_0$  field along  $\hat{z}$ , a defect with symmetry axis along  $\hat{x}$  will have a transition strength proportional to  $(\langle H_{ix}^2 \rangle + 4\langle H_{iy}^2 \rangle)$ , while the  $\hat{y}$  oriented defect signal will go as  $(\langle H_{iy}^2 \rangle + 4\langle H_{ix}^2 \rangle)$ . The angle brackets indicate averages over the sample. Because the sample has (slightly) perturbed the cavity mode there is some uncertainty about the ratio  $\langle H_{ix}^2 \rangle / \langle H_{iy}^2 \rangle$ . This ratio can be determined experimentally by exploiting the incidental presence of the equally populated  $x$  and  $y$  oriented  $\text{Fe}^{3+}\text{-}V_0$  defects in our samples, where an analogous asymmetry in transition strength serves to calibrate the microwave field distribution. It is then straightforward to correct the raw data from the  $\text{Fe}^{1+}\text{-}V_0$  system so that it directly reflects the population ratios.

Labeling the two lines of Fig. 8(a)  $A$  and  $B$ , and expressing the polarization dependence of the relative signals as

$$P = \frac{I_A - I_B}{I_A + I_B} \quad (14)$$

where the intensities of  $A$  and  $B$  ( $I_A$  and  $I_B$ ) have been corrected for both transition probability differences and microwave field configuration, the polarization dependence for light with the polarization vector perpendicular to both centers is shown in Fig. 8(b). The approximately zero polarization dependence for all wavelengths is expected.

However, if the polarization vector of the light is such that it is parallel to one defect axis (the  $A$  signal) and perpendicular to the other (the  $B$  signal) the ESR trace of Fig. 8(c) results for optical pumping at 400 nm. Comparing with Fig. 8(a), which represents equal  $A$  and  $B$  intensities, the greatly increased intensity of the  $A$  line demonstrates an enhanced production of centers with defect axes parallel to the pumping light polarization direction. Figure 8(d) is a plot of  $P$  [see Eq. (14)] as a function of wavelength for this second geometry. Clearly,  $A$  centers are preferentially created by blue light and  $B$  centers are preferentially created by green light. A simple model for this unusual result will be presented in Sec. IV A.

Assuming the  $\text{Fe}^{1+}\text{-}V_0$  is created from  $\text{Fe}^{2+}\text{-}V_0$  then there are only two possible mechanisms for this production. Either  $\text{Fe}^{2+}\text{-}V_0$  captures an electron freed by the optical pumping, or an electron is directly excited by the optical pumping into the  $\text{Fe}^{2+}\text{-}V_0$  from the valence band. If the production were by electron capture there should be no polarization effect because all of the  $\text{Fe}^{2+}\text{-}V_0$  defects would have the same probability of capturing an electron and the relative populations of the  $A$  and  $B$  centers would al-

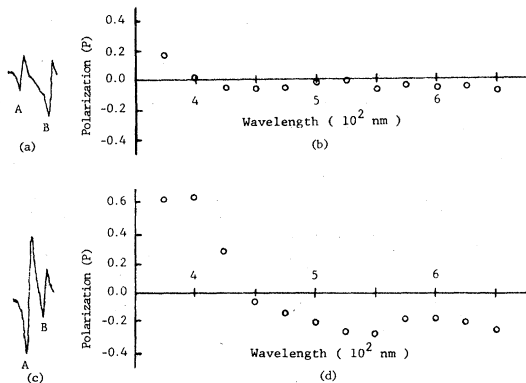


FIG. 8. (a) ESR trace of two geometrically inequivalent  $\text{Fe}^{1+}\text{-}V_0$  centers produced by light at 400 nm. The light is polarized perpendicular to the tetragonal axis of both. (b) The normalized polarization ratio of the  $A$  and  $B$  centers  $P = (I_A - I_B)/(I_A + I_B)$  as a function of  $\lambda$  for light polarized perpendicular to both centers. No polarization result is expected. (c) Same as (a) except for a  $90^\circ$  rotation of the polarization of the incident light. The polarization axis is parallel to  $A$  defects and perpendicular to  $B$  defects, showing the preferential population of the  $A$  defects. (d) The normalized polarization ratio of the  $A$  and  $B$  center as a function of  $\lambda$ . For short wavelengths  $A$  centers are preferentially produced, and for long wavelengths  $B$  centers are preferentially produced.

ways be equal. Therefore the polarization dependent production of the  $\text{Fe}^{1+}\text{-}V_0$  defects must represent the direct excitation of an electron from the valence band onto  $\text{Fe}^{2+}\text{-}V_0$ .

### C. Kinetics

The kinetics may be interpreted by the simple model illustrated in Fig. 7. The production is through the direct excitation of a valence electron into  $\text{Fe}^{2+}\text{-}V_0$  creating  $\text{Fe}^{1+}\text{-}V_0$  while the resulting hole is captured by  $\text{Fe}^{2+}\text{-}I$  creating  $\text{Fe}^{3+}\text{-}I$ . Qualitatively this model explains the appearance of the  $\text{Fe}^{1+}\text{-}V_0$  at the same rate as the  $\text{Fe}^{3+}\text{-}I$ . An absolute conversion efficiency has not been determined because of complications in the microwave transition matrix elements of the  $\text{Fe}^{3+}\text{-}I$  centers, but the measurements are consistent with a production ratio of unity.

If the optical decay process also proceeds through

direct excitation of an electron from the valence band, and subsequent migration of the hole, the kinetics of optical production and optical decay should be related. In both cases these kinetics are determined by the competition of the same two centers ( $\text{Fe}^{1+}\text{-}V_0$  and  $\text{Fe}^{2+}\text{-}I$ ) for capturing a hole.

In the case at hand these kinetics are particularly simple because the ESR signals tell us that the number of  $\text{Fe}^{2+}\text{-}V_0$  centers is much greater than the total number of interstitial sites. This means the  $\text{Fe}^{2+}\text{-}V_0$  system can be treated as an infinite reservoir. The optical production process will saturate when all interstitial sites are converted to the  $\text{Fe}^{3+}\text{-}I$  state, and all holes liberated after that time must be retrapped by  $\text{Fe}^{1+}\text{-}V_0$  centers.

Converting the observed signal,  $x$  (either the  $\text{Fe}^{1+}\text{-}V_0$  or the  $\text{Fe}^{3+}\text{-}I$  signal) into dimensionless normalized units by dividing by the saturation signal, it is straightforward to show that the shape of the optical

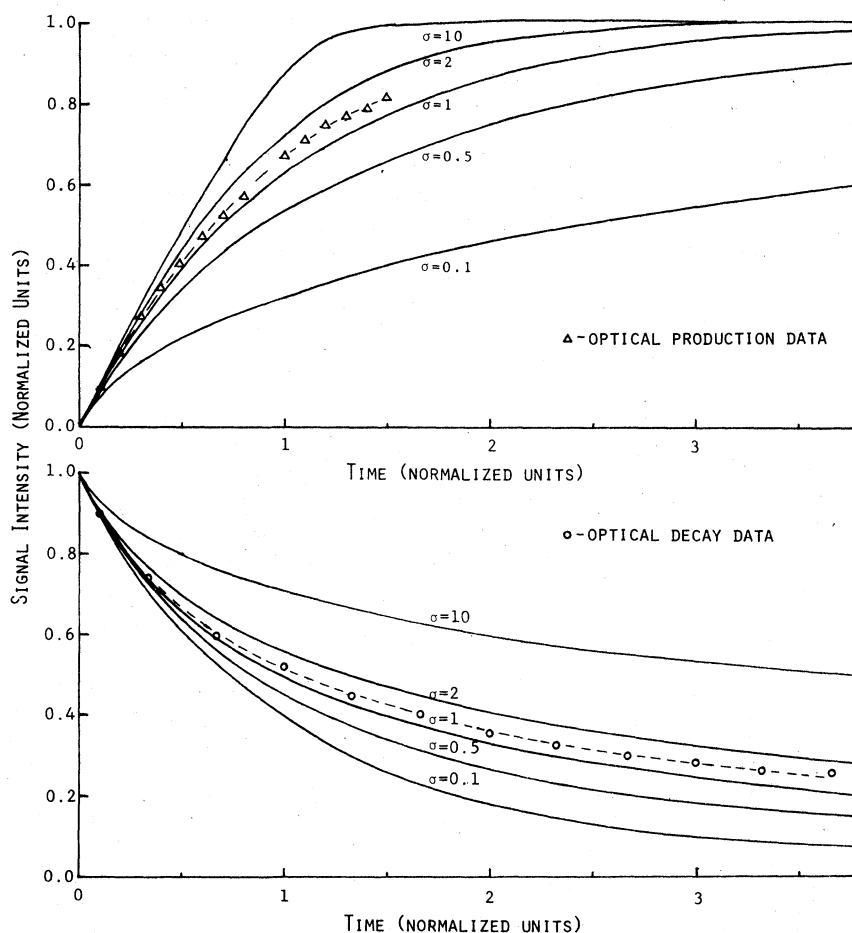


FIG. 9. The solid lines for the optical production (upper curves) and optical decay (lower curves) were produced from Eqs. (15) and (16), respectively, by varying  $\sigma$ , the hole-capture cross-section ratio of  $\text{Fe}^{2+}\text{-}I$  to  $\text{Fe}^{1+}\text{-}V_0$ . A  $\sigma$  of 1.5 fits both the optical production data ( $\Delta$  points) and optical decay data ( $\circ$  points).

production curve as a function of time is given by

$$\left(\frac{dx}{dt}\right)_{\text{production}} = \frac{(1-x)\sigma}{x + (1-x)\sigma}, \quad x(0) = 0, \quad (15)$$

where the time axis has been arbitrarily rescaled to given an initial slope of unity, and  $\sigma = \sigma(\text{Fe}^{2+}/\sigma(\text{Fe}^{1+}-V_0))$  is the ratio of hole capture cross sections.

The corresponding result for the optical decay process, with illumination in the near ir driving valence electrons into the  $\text{Fe}^{3+}/I$  center, is

$$\left(\frac{dx}{dt}\right)_{\text{decay}} = \frac{-x^2}{x + (1-x)\sigma}, \quad x(0) = 1. \quad (16)$$

These equations are plotted in Fig. 9 for a range of values for  $\sigma$ , and the experimentally determined production and decay curves, rescaled to the appropriate initial slope, are superimposed.

The curves show that there exists a  $\sigma$  for each curve which will fit the experimental data. More importantly, the same value of  $\sigma$  ( $\approx 1.5$ ) fits both curves, confirming the model illustrated in Fig. 7. The near equality of the hole capture cross sections suggests that both the trapping sites  $\text{Fe}^{1+}-V_0$  and  $\text{Fe}^{2+}/I$  have the same electric charge with respect to the neutral lattice. This is the evidence alluded to at the end of Sec. II A that the interstitial has a charge of  $+1$ . For both optical production and optical decay the hole is then excited out of an electrically neutral system (with respect to the unperturbed lattice) and captured by a system with net charge  $-1$ .

#### IV. DISCUSSION

##### A. Polarization effects

The production of preferentially oriented  $\text{Fe}^{1+}-V_0$  systems by the use of polarized light, as described in Sec. III B, is direct evidence that the optical transition involves excitation of a valence electron into the localized  $\text{Fe}^{2+}-V_0$  site. We have not attempted to analyze this effect in detail by calculating transition probabilities, but it is straightforward to show that the sign and overall shape of the polarization response are plausible, by considering the charge-transfer bands of an  $\text{FeO}_5$  molecular cluster.

We need to consider the transition matrix element

$$\langle \psi_f | H_{\text{int}} | \psi_i \rangle, \quad (17)$$

where we assume  $H_{\text{int}}$  to be the standard electric dipole operator proportional to  $\sum_i \vec{r}_i$ , with  $i$  running over all electrons. The initial state is an antisymmetrized product function for a seven-electron system consisting of the six  $3d$  electrons localized on the

$\text{Fe}^{2+}$  ion, and one valence-band electron. The one electron  $d$  orbitals are uniquely defined for the  ${}^5B_2$  ground state of Fig. 4, so that

$$|\psi_i\rangle = |\theta^+ \epsilon^+ \zeta^2 \xi^+ \eta^+\rangle |v\rangle, \quad (18)$$

where  $|v\rangle$  is a valence-band electron, and the notation for the  $d$  orbitals is standard. The final state must be one of the spin quartets of the seven-electron system  $\text{Fe}^{1+}$ . The  ${}^4A_2$  ground state shown in Fig. 6 looks like

$$\langle \theta^+ \epsilon^+ \xi^2 \eta^2 \zeta^+ | + \alpha \langle \xi^+ \eta^+ \zeta^2 \epsilon^2 \theta^+ |, \quad (19)$$

where  $\alpha$  is an admixture coefficient which depends on the ratio of the Racah  $B$  parameter to the cubic field splitting  $\Delta$ . This  $\alpha$  will be small, and vanishes in the strong crystal-field limit. If we neglect  $\alpha$ , then there will be no transition strength at all to the  $\text{Fe}^{1+}$  ground state because it differs in the coordinates by more than one electron from the initial state, and  $H_{\text{int}}$  is a sum of one-electron operators. There is a low-lying excited orbital doublet, though ( ${}^4E$  in Fig. 6) with configurations that are mainly

$$\langle \theta^+ \epsilon^+ \eta^2 \zeta^2 \xi^+ |, \quad \langle \theta^+ \epsilon^+ \zeta^2 \eta^+ \xi^2 |, \quad (20)$$

that can be directly connected with the initial state, and we assume this is the relevant final state for the optical pumping. The transition matrix elements are now governed by

$$\langle \xi^- | \vec{r} | v^- \rangle \text{ and } \langle \eta^- | \vec{r} | v^- \rangle \quad (21)$$

and the one-electron picture for the optical transition is sketched in Fig. 10(a).

As a rough guide to the distribution of valence-band states we can take the oxygen  $2p$  cluster levels for the  $\text{TiO}_5$  cluster, as given by Wolfram *et al.*<sup>20</sup> These levels are shown in Fig. 10(b) labeled in the appropriate  $C_{4v}$  symmetry. The final-state  $d$  orbitals  $t_{2\xi}$  and  $t_{2\eta}$  are also shown on this diagram. The allowed transitions and their polarizations follow directly from the  $C_{4v}$  character table.

The first transition to appear as the frequency of the exciting light is increased from zero would be the transition from the upper  $A_2$  cluster level, and this transition could only appear in those centers whose vacancy axis lies perpendicular to the electric field vector. About 0.5 eV higher in energy this transition is replaced by that from the upper  $E$  cluster level, and now only parallel orientations are excited. This scheme is precisely the one observed experimentally. One could look deeper into the valence band or higher in the local Fe excited states, of course. Banding is clearly important in these optical transitions since they are all quite broad, and covalency effects are likely to be important in any actual calculation of the oscillator strengths. It is gratifying though that the simplest possible interpretation seems to give good agreement with the observed behavior.

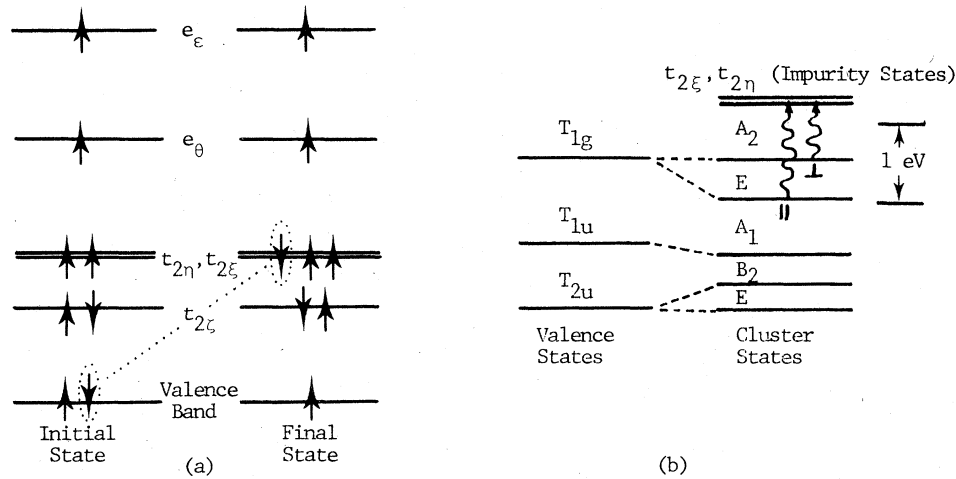


FIG. 10. (a) The initial and final electron configurations for the optical pumping showing the transfer of an electron from the valence band to the  $t_{2g}$ , or  $t_{2g}$  level. (b) The allowed optical transitions from the valence  $A_2$  and  $E$  band states to the  $Fe^{2+}-V_0$  impurity state, and the polarization of light with respect to the impurity  $z$  axis which drives these transitions. The transitions of (b) are consistent with the observed polarization dependent production of  $Fe^{1+}-V_0$  centers.

**B. Crystal field at the  $Fe-V_0$  site**

In Sec. II the spin-Hamiltonian parameters for  $Fe^{2+}-V_0$  and  $Fe^{1+}-V_0$  were analyzed with the tacit assumption of a well localized  $(3d)^n$  ion perturbed by a crystal field of  $C_{4v}$  symmetry. If we include the previously identified defects  $Fe^{3+}-V_0$  and  $Fe^{4+}-V_0$ , then ESR data are available for four different charge states of Fe, all in the identical fivefold coordinated site. It appears that a "universal" crystal field can be associated with this site that is compatible with all the ESR results for all four ions.

This crystal field may be conveniently parametrized by its effect on a set of (hypothetical) one-electron  $3d$  orbitals as illustrated by the  $d$ -orbital pattern shown in Fig. 11. The degeneracies are determined by the symmetry, but the qualitative level splittings are meant to agree with a model originally suggested by Griffith to account for the properties of fivefold coordinated metal porphyrins and hemoglobin derivatives.<sup>21</sup> According to Griffith the splitting of the  $t_{2g}$  levels is small ( $\delta < 5 \times 10^3 \text{ cm}^{-1}$ ), the  $\epsilon$  level is very high ( $2 \times 10^4 \text{ cm}^{-1}$ ), and the  $\theta$  level is down near the  $t_{2g}$ 's, but above them. The connection between these one-electron orbital energies and those aspects of the true many electron eigenstates that are observable is given below.

**1.  $\epsilon$**

Schirmer *et al.*<sup>9</sup> have shown that the ground state of  $Fe^{4+}-V_0$  is a high spin ( $S = 2$ ) orbital singlet, with a fine-structure splitting  $D < 0$ . This corresponds to occupying the four lowest levels in Fig. 11 to form a  $^5B_1$  ground state. The energy-level diagram for  $Fe^{4+}-V_0$  is not given, but it would correspond to an

inversion of Fig. 4. If  $\epsilon$  were below  $\theta$  the lowest state would be  $^3A_1$  rather than  $^5B_1$  and  $D$  would be greater than zero contradicting experiment.

The high-spin ground state for  $Fe^{2+}-V_0$  is independent of the relative energies of the  $\epsilon$  and  $\theta$  levels, but the spin-Hamiltonian parameters  $D$  and  $g_{||}$  of Eq. (10) suggest that the  $^5B_1$  level of Fig. 4 is very high. The energy splitting to this level ( $W_2$  in Fig. 4) corresponds exactly to the energy of the  $\epsilon$  level in Fig. 11, so a large value for  $W_2$  is expected from Griffith's model.

**2.  $\theta$**

Switching the  $\theta$  level of Fig. 11 below the  $t_{2g}$ 's alters the ground states for both  $Fe^{2+}-V_0$  and  $Fe^{1+}-$

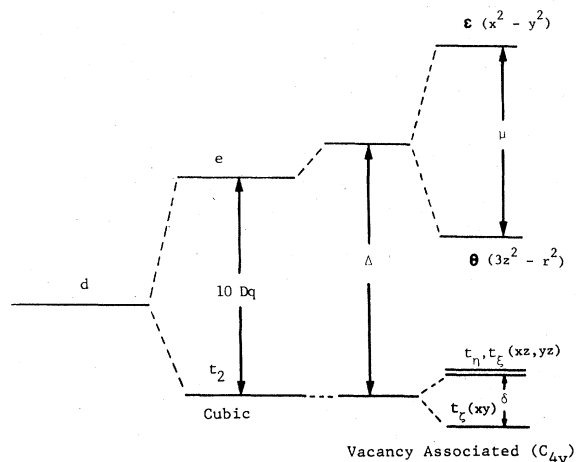


FIG. 11. Energy-level diagram for a  $3d$  electron at a site of  $C_{4v}$  symmetry.

$V_0$ . For  $\text{Fe}^{2+}-V_0$  the new ground state is unambiguously the  ${}^5A_1$  of Fig. 4 and it is straightforward to show this leads to inconsistencies between  $\delta g_{\parallel}$  and  $D$ . Perturbation theory to the same order as in Eq. (10) yields  $D = 3\lambda^2/W_1'$  and  $g_{\parallel} = 2 - 3(\lambda/W_1')^2$ , where  $W_1'$  is the energy splitting from the ground  ${}^5A_1$  to the  ${}^5E$ . Inserting the experimental numbers yields  $|\lambda| \approx 32$  cm, which is much too small for an Fe ion. The  $\text{Fe}^{1+}-V_0$  case is more complicated, but the  ${}^4A_2$  level (Fig. 6) is the only low-lying state consistent with the measured  $g_{\parallel} = 1.999$ , all other levels in the ground multiplet having positive contributions to  $\delta g_{\parallel}$  in a low order of perturbation theory.

### 3. $\delta$

Numerical values for the parameter  $\delta$  in Fig. 11 can be determined from both  $\text{Fe}^{2+}-V_0$  and  $\text{Fe}^{1+}-V_0$ . The  $\text{Fe}^{2+}-V_0$  case is trivial, since  $\delta = W_1 \approx +800$   $\text{cm}^{-1}$ . For  $\text{Fe}^{1+}-V_0$  to a first approximation  $-\delta \approx W \approx 3500$   $\text{cm}^{-1}$ . This requires some correction because  $W$  is not independent of  $\Delta$  and  $\mu$ , but the correction is not very great for reasonable values of these parameters and a  $\delta \approx -4000$   $\text{cm}^{-1}$  is probably about right. The magnitude of  $\delta$  is plausible for both ions, but to be consistent with Fig. 11 we require a change in sign on going from  $(3d)^6$  to  $(3d)^7$ . This is not particularly surprising, since even in a trivial point-charge calculation the smallness of  $\delta$  is due to partial cancellation between two larger terms.

### 4. $\text{Fe}^{3+}-V_0$

The  $\text{Fe}^{3+}-V_0$  spectrum provides some independent evidence supporting the orbital pattern of Fig. 11. This ion has an axial fine structure  $D = +1.31$   $\text{cm}^{-1}$ . There is also a fourth-order fine-structure term in the spin Hamiltonian,  $a_t = 133 \times 10^{-4}$   $\text{cm}^{-1}$  measured by Pontin *et al.*<sup>22</sup> and verified by us using a different set of transitions. The corresponding fourth-order term for a  $\text{Fe}^{3+}$  ion at a cubic site is  $a_c = 198 \times 10^{-4}$   $\text{cm}^{-1}$ . These two defects differ only by the removal of one of the six ligand oxygens, and it is reasonable to suppose that the major effect is to sharply reduce the energy of the  $\theta$  level, as in Fig. 11. This conjecture turns out to be consistent both with the appearance of the second-order term  $D$ , and the observed change in the fourth-order term  $a_c - a_t$ .

To show this, we fit the observed  $a_c$  in the cubic site to a consistent set of parameters (10 Dq, Racah  $B$  and  $C$ , and spin-orbit  $\zeta$ ) using the numerical results of Gabriel *et al.*<sup>23</sup> The effect of lowering the  $\theta$  level is then computed from the perturbation analysis of Golding and Singhasavich.<sup>24</sup> The results are plotted in Fig. 12, for initial values of 10 Dq = 18000  $\text{cm}^{-1}$ ,  $B = 800$   $\text{cm}^{-1}$ ,  $C = 4.5B$ , and  $\zeta = 413$   $\text{cm}^{-1}$ . The single value  $\mu \approx 11000$   $\text{cm}^{-1}$  accounts reasonably well for both fine-structure parameters of the  $\text{Fe}^{3+}-V_0$

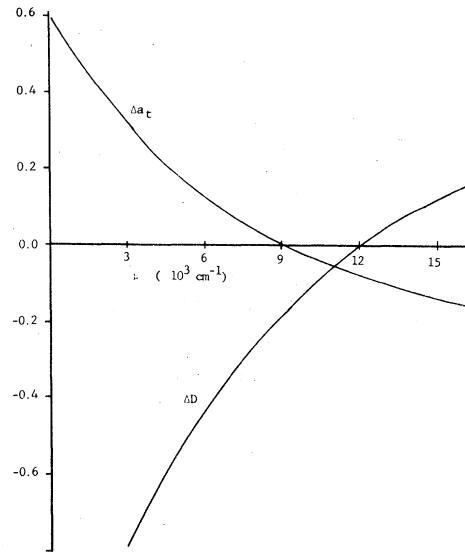


FIG. 12. A comparison of calculated crystal-field parameters  $a_t$  and  $D$  as a function of  $\mu$  (the one-electron  $\epsilon$  and  $\theta$  splitting), and the measured  $a_t$  and  $D$  for  $\text{Fe}^{3+}-V_0$ .  $\Delta a_t = [a_t(\text{calc}) - a_t(\text{expt})]/a_t(\text{calc})$  and  $\Delta D = [D(\text{calc}) - D(\text{expt})]/D(\text{calc})$ .

system. This conclusion remains qualitatively true for any reasonable set of initial parameters that gives the proper value for  $a_c$ .

### C. Multiple charge states

The appearance of the  $\text{Fe}^{1+}-V_0$  complex in these crystals was initially something of a surprise to us. Since the state is stable indefinitely at reduced temperature, it must correspond to a level in the crystal band gap. Including the  $\text{Fe}^{4+}-V_0$  system then, the 3.2-eV band gap of pure  $\text{SrTiO}_3$  contains at least four stable charge states for the Fe atom in the identical  $\text{Fe}-V_0$  complex. One way to illustrate this situation is sketched in Fig. 13, where the levels drawn indicate the charge state of the local system as a function of the position of the Fermi level.

On physical grounds, though, consecutive local impurity levels, as shown in Fig. 13, should be separated by an energy  $U$  equal to the interaction energy between a pair of  $d$  electrons localized on the Fe atom. A naive estimate of this energy based on absolute free-ion energy levels gives values for  $U$  in the neighborhood of 10 eV, at least an order of magnitude too large.

This collapse of the local impurity charge states in a crystal is a well-known phenomenon, particularly in semiconductors where the effects can be dramatic. Haldane and Anderson have shown that the main driving term for producing the collapse in a semiconductor is delocalization of the  $d$ -electron charge densi-

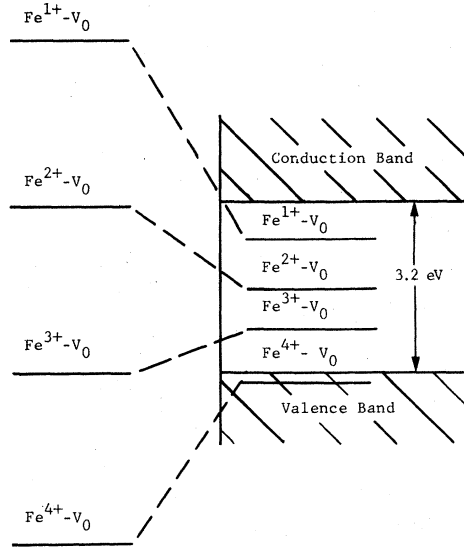


FIG. 13. A diagram of the Fe- $V_0$  levels showing the large free-ion energy separation and the greatly reduced energy difference in the crystal lattice.

ty.<sup>25</sup> In a metal, on the other hand, Herring has shown that free-electron screening can reduce  $U$  by a large factor.<sup>26</sup>

In an ionic crystal like SrTiO<sub>3</sub>, where screening is absent and delocalization is not likely to be great, it seems natural to investigate the electrostatic energy associated with polarization of the lattice around the impurity. The following simple model calculation confirms that this can indeed be an important effect.

Consider the energy of an isolated Fe ion consisting of an argon core plus  $n$  electrons in the  $d$  shell. (For the neutral atom then,  $n = 8$ .) This can be parametrized by

$$E_{\text{atom}} = -nE_d + \frac{1}{2}Un(n-1) \quad (22)$$

In a crude sense  $E_d$  could be considered a Hartree-Fock energy for the  $d$  shell, and  $U$  a  $d$ - $d$  correlation energy, but this interpretation is inaccurate and unnecessary. Experimentally the first three ionization potentials<sup>27</sup> for Fe are 7.6, 16.18, and 30.64 eV, and if we choose  $E_d = +80$  eV and  $U = +10$  eV, Eq. (22) gives 10, 20, and 30 eV for these ionization potentials, for a reasonable fit. Small effects due to multiplet structure and alternative  $n$ -electron configurations are ignored.

If a neutral Fe atom is substituted on a Ti site in the lattice, and some of the electrons are allowed to go to the Fermi level, then the dependence of the total energy on  $n$ , the number of localized  $d$  electrons, is given by

$$E_{\text{tot}} = E_{\text{atom}} + (8-n)E_m + (8-n)E_F \quad (23)$$

where  $E_m$  is a Madelung energy ( $-32$  eV at a

vacancy-associated site<sup>28</sup>) and  $E_F$  is the Fermi energy. Minimization of Eq. (23) leads to an equilibrium number of  $d$  electrons

$$n = (E_d + E_m + E_F + \frac{1}{2}U)/U \quad (24)$$

and a level spacing between consecutive charge states in the band gap of

$$(dn/dE_F)^{-1} = U \quad (25)$$

as expected.

Such a calculation may make some sense, but only if the net polarization surrounding the lattice is relatively small. If the impurity ion charge differs from +4 (the neutral state with respect to the lattice), then dipoles are induced in the surrounding lattice, lowering the total energy of the system. We can account for this energy by adding a term of the form

$$E_d = -\frac{1}{2}(n-4)^2|e||V| \quad (26)$$

to Eq. (23), where  $V$  is the reaction potential at the impurity site due to the dipoles induced by a unit charge discrepancy. Including this term in the total energy [Eq. (23)] reduces the stabilizing influence of  $U$  for selecting a particular charge state, so that

$$\left(\frac{dn}{dE_F}\right)^{-1} = U - |e||V| \quad (27)$$

If  $V$  can approach 10 V, the local system is on the verge of being unstable to charge transfer.

The evaluation of  $V$  is an awkward self-consistent electrostatics problem, particularly in the perovskite lattice, where the oxygen sites lack cubic symmetry. It is possible, though, to make a plausible estimate along the lines of a calculation by Mott and Littleton.<sup>29</sup>

Within the crystal we know

$$D = \epsilon E = \epsilon_0 E + P = e/4\pi r^2 \quad (28)$$

If only the oxygen moments contribute to the polarization, then

$$P = 3\mu_{\text{ox}}/8a^3 \quad (29)$$

where  $\mu_{\text{ox}}$  is the average radial dipole moment and  $2a$  is the unit cell length. Combining Eq. (29) with Eq. (28)

$$\mu_{\text{ox}} = \frac{8a^3 e (1 - \epsilon_0/\epsilon)}{12\pi r^2} \quad (30)$$

Mott and Littleton's zeroth-order approximation is to assume this expression holds at all lattice sites.

The change in potential at the origin will be

$$V_i = \frac{-\mu_{\text{ox}}}{4\pi\epsilon_0 r_i^2} \quad (31)$$

and combining with Eq. (30) gives

$$V = \frac{-e(1 - \epsilon_0/\epsilon)}{6\pi^2\epsilon_0a} \sum_i \left( \frac{a}{r_i} \right)^4. \quad (32)$$

For SrTiO<sub>3</sub>,  $2a = 3.9051 \text{ \AA}$ ,  $\epsilon/\epsilon_0 \approx 5$  (electronic polarizability only), and  $\sum_i (a/r_i)^4 \approx 8.8$  for the perovskite lattice. This gives  $V = 11 \text{ V}$ , and in our simple model the polarization reaction has completely canceled the stabilizing influence of the electron-electron interaction energy  $U$ . This result is more or less specific to the perovskite lattice. An analogous calculation in MgO or KCl leads to significantly smaller values for  $V$ , and well-spaced intervals between alter-

nate charge states of transition ion impurities.

This model calculation is admittedly naive, but it has the virtue of no adjustable parameters, and we feel it correctly identifies an essential feature of the problem.

#### ACKNOWLEDGMENTS

We would like to thank Dr. Frank Morin for stimulating our interest in this problem, and providing us with samples. Several helpful conversations with Professor Thomas Wolfram are gratefully acknowledged.

\*Present address: Dept. of Phys., Univ. of Dayton, Dayton, Ohio 45469.

<sup>1</sup>K. A. Müller, *Helv. Phys. Acta* **31**, 173 (1958).

<sup>2</sup>R. A. Serway, W. Berlinger, K. A. Müller, and R. W. Collins, *Phys. Rev. B* **16**, 4761 (1977).

<sup>3</sup>E. S. Kirkpatrick, K. A. Müller, and R. S. Rubins, *Phys. Rev.* **135**, A86 (1964).

<sup>4</sup>H. Unoki and T. Sakudo, *J. Phys. Soc. Jpn.* **23**, 546 (1967).

<sup>5</sup>K. A. Müller, W. Berlinger, and R. S. Rubins, *Phys. Rev.* **186**, 361 (1969).

<sup>6</sup>B. W. Faughman, *Phys. Rev. B* **4**, 3623 (1971).

<sup>7</sup>O. Koidl, K. W. Blazey, W. Berlinger, and K. A. Müller, *Phys. Rev. B* **14**, 2703 (1976).

<sup>8</sup>Z. J. Kiss, *Phys. Today* **23**, 42 (1970).

<sup>9</sup>O. F. Schirmer, W. Berlinger, and K. A. Müller, *Solid State Commun.* **16**, 1289 (1975).

<sup>10</sup>K. A. Müller, Th. Von Waldkirch, and W. Berlinger, *Solid State Commun.* **9**, 1097 (1971).

<sup>11</sup>Th. W. Kool and M. Glasbeck, *Solid State Commun.* **22**, 193 (1977).

<sup>12</sup>R. L. Berney, D. L. Cowan, and F. Morin, *Solid State Commun.* **26**, 579 (1978). The Fe- $I$  system was denoted Fe<sub>th</sub><sup>3+</sup> in this preliminary description of the ESR results. Additional ESR transitions have been observed and are discussed in this paper.

<sup>13</sup>R. D. Dowsing and F. J. Gibson, *J. Chem. Phys.* **50**, 294 (1969).

<sup>14</sup>O. F. Schirmer and K. A. Müller, *Phys. Rev. B* **7**, 2986 (1973).

<sup>15</sup>A. Abragam and B. Bleaney, *Electron Paramagnetic Resonance of Transition Ions* (Clarendon, Oxford, 1970), (a) p. 209, (b) p. 110.

<sup>16</sup>M. Tinkham, *Proc. R. Soc. London Ser. A* **236**, 535 (1956).

<sup>17</sup>U. Kaufmann, *Phys. Rev. B* **14**, 1848 (1976).

<sup>18</sup>J. S. Griffith, *The Theory of Transition Metal Ions* (Cambridge University Press, Cambridge, 1961), p. 355.

<sup>19</sup>A. Abragam and M. H. L. Pryce, *Proc. R. Soc. London Ser. A* **206**, 164 (1951).

<sup>20</sup>T. Wolfram, R. Hurst, and F. J. Morin, *Phys. Rev. B* **15**, 1151 (1977).

<sup>21</sup>See Ref. 18, p. 371.

<sup>22</sup>R. G. Pontin, E. F. Slade, and D. J. E. Ingram, *J. Phys. Chem.* **2**, 1146 (1969).

<sup>23</sup>J. R. Gabriel, D. F. Johnson, and M. J. D. Powell, *Proc. R. Soc. London Ser. A* **264**, 503 (1969).

<sup>24</sup>R. M. Golding and T. Singhasavich, *Mol. Phys.* **29**, 1847 (1975).

<sup>25</sup>F. D. M. Haldane and P. W. Anderson, *Phys. Rev. B* **13**, 2553 (1976).

<sup>26</sup>C. Herring, in *Magnetism*, edited by G. T. Rado and H. Suhl (Academic, New York, 1966), Vol. IV, pp. 190–200.

<sup>27</sup>See Ref. 18, p. 379.

<sup>28</sup>E. A. Kraut, T. Wolfram, and W. Hall, *Phys. Rev. B* **6**, 1499 (1972).

<sup>29</sup>W. F. Mott and M. J. Littleton, *Trans. Faraday Soc.* **34**, 485 (1938).